LETTERS

Genome-wide localization of small molecules

Lars Anders[1,6], Matthew G Guenther[1,6], Jun Qi[2], Zi Peng Fan[1,3], Jason J Marineau[2], Peter B Rahl[1], Jakob Lovén[1], Alla A Sigova[1], William B Smith[2], Tong Ihn Lee[1], James E Bradner[2,4] & Richard A Young[1,5]

A vast number of small-molecule ligands, including therapeutic drugs under development and in clinical use, elicit their effects by binding specific proteins associated with the genome. An ability to map the direct interactions of a chemical entity with chromatin genome-wide could provide important insights into chemical perturbation of cellular function. Here we describe a method that couples ligand-affinity capture and massively parallel DNA sequencing (Chem-seq) to identify the sites bound by small chemical molecules throughout the human genome. We show how Chem-seq can be combined with ChIP-seq to gain unique insights into the interaction of drugs with their target proteins throughout the genome of tumor cells. These methods will be broadly useful to enhance understanding of therapeutic action and to characterize the specificity of chemical entities that interact with DNA or genome-associated proteins.

The ability to map the locations of proteins throughout the genome has had a profound impact on our understanding of a wide range of normal and disease biology. For example, discovery of the genome-wide location of proteins by means of chromatin immunoprecipitation (ChIP)-seq has allowed global mapping of the key transcription factors and chromatin regulators that control gene expression programs in various cells, the sites that act as origins of DNA replication, and regions of the genome that form euchromatin and heterochromatin[1–6]. Models of the transcriptional regulatory circuitry that controls normal and disease states in cells have emerged from genome-wide data[7–10].

Mapping the global interactions of a chemical entity with chromatin genome-wide could provide insights into the mechanisms by which a small molecule influences cellular functions. Many DNA-associated processes are targeted for disease therapy, including transcription, modification, replication and repair[11–16]. Ligand-affinity methodologies have greatly contributed to our understanding of drug and ligand function, and have led to the identification of numerous gene regulatory drug targets[17–20]. There have been initial efforts to map the sites of interaction of metabolic compounds in the yeast genome[21], but it would be ideal to have a method that allows investigators to determine how small-molecule therapeutics interact with the human genome. We describe here a method based on chemical affinity capture and massively parallel DNA sequencing (Chem-seq) that allows investigators

to identify genomic sites where small chemical molecules interact with their target proteins or DNA (**Fig. 1a**). The Chem-seq method is similar to that employed for ChIP-seq, except that Chem-seq uses retrievable synthetic derivatives of a compound of interest to identify sites of genome occupancy whereas ChIP-seq uses antibodies against specific proteins for this purpose.

We used Chem-seq to investigate the genome-wide binding of the bromodomain inhibitor JQ1 to the BET bromodomain family members BRD2, BRD3 and BRD4 in MM1.S multiple myeloma cells. JQ1 has previously been shown to bind all three co-activator proteins and to inhibit the growth of MM1.S and other tumor cells[13,22–27]. We first investigated how BRD2, BRD3 and BRD4 occupy the genome of MM1.S cells using ChIP-seq (**Supplementary Fig. 1**). All three proteins were found to be associated with actively transcribed genes (**Supplementary Fig. 1a**). Inspection of individual gene tracks (**Supplementary Fig. 1b**) and analysis of global genome occupancy (**Supplementary Fig. 1c**) showed that most core promoter elements of active genes were co-occupied by BRD2, BRD3 and BRD4 together with RNA polymerase II (RNA Pol II), the Mediator complex subunit 1 (MED1) and histone H3K27Ac. In contrast, enhancers, which are occupied by histone H3K27Ac and Mediator, were preferentially occupied by BRD4, with lower relative levels of BRD2 and BRD3.

To investigate the interaction of JQ1 with chromatin genome-wide, we used the Chem-seq technique (**Fig. 1a**) with a biotinylated derivative of JQ1 (bio-JQ1, **Fig. 1b**). Enantioretentive substitution at C-6 of the JQ1 diazepine allowed coupling of a polyethylene glycol spacer with appended biotin feature. The potency of bio-JQ1 binding to the first bromodomain of BRD4 was nearly equivalent to that of the unbiotinylated compound, as determined by both differential scanning fluorimetry and isothermal titration calorimetry (**Supplementary Fig. 2**). Consistent with this, bio-JQ1 had only slightly reduced bioactivity in MM1.S cells relative to JQ1 (**Fig. 1c**). We initially treated living cells with bio-JQ1 and cross-linked proteins to DNA with formaldehyde (**Fig. 1a**). Cells were then lysed and sonicated to shear the DNA, and streptavidin beads were used to isolate biotinylated ligand and associated chromatin fragments. Massively parallel sequencing was used to identify enriched DNA fragments, and these sequences were mapped to the genome to reveal sites bound by the small-molecule probe.

In addition, we developed an *in vitro* version of this method, which allows analysis of biotinylated molecules with potentially
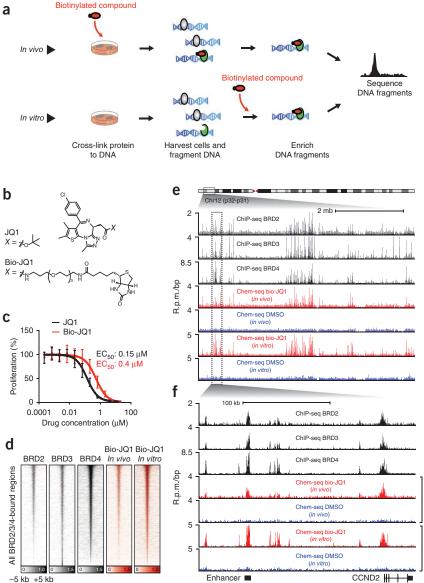
Figure 1 Chem-seq from intact cells or cellular lysates reveals genomic sites bound by the BET bromodomain-targeting drug JQ1. (**a**) Features of the Chem-seq method in living cells (*in vivo*, top) and cell lysates (*in vitro*, bottom). Top: cells are treated with a biotinylated drug to allow drug-target binding. Formaldehyde treatment cross-links chromatin-associated proteins to DNA, including drug-target complexes associated with chromatin. After cell lysis and sonication, DNA fragments bound to the drug-target complex are enriched using streptavidin beads. Sequencing of the enriched DNA fragments permits genome-wide identification of the loci to which the drug target binds. Bottom (*in vitro*): the biotinylated drug is added to the cell extract, where it binds protein-DNA complexes. Enrichment of DNA fragments and sequencing is carried out as in the *in vivo* method. (**b**) Chemical structures of JQ1 and its biotinylated version, bio-JQ1. (**c**) Effect of JQ1 (black) and bio-JQ1 (red) on MM1.S cell proliferation. Cells were treated with varying concentrations of drug for 72 h. Error bars, mean ± s.d. (**d**) Heatmap representation of binding of the individual BET proteins (ChIP-seq, black) and bio-JQ1 (*in vivo* and *in vitro* Chem-seq, red) to the union of all 25,450 regions occupied by BRD2, BRD3, BRD4 and bio-JQ1. Read density surrounds the center (±5 kb) of all occupied regions, rank ordered from highest to lowest BRD4 occupancy. (**e**) Gene tracks showing BRD2, BRD3, BRD4 and bio-JQ1 occupancy of a region of chromosome 12. ChIP-seq reads for BRD2, BRD3 and BRD4 (black), Chem-seq reads for biotinylated JQ1 (bio-JQ1, red) or DMSO vehicle control (blue) are shown. The genome-wide data are plotted in reads per million per base pair (r.p.m./bp). (**f**) Close-up view of gene tracks showing BRD2, BRD3 and BRD4 occupancy (ChIP-seq) and bio-JQ1 occupancy (Chem-seq) across the CCND2 gene locus.
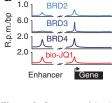

limited cell permeability (**Fig. 1a**). To this end, MM1.S cells were fixed and the derived sonicated lysate incubated with biotinylated JQ1 to enrich for bound chromatin regions *in vitro*.

We found that both *in vivo* and *in vitro* Chem-seq produced essentially the same result: the genomic sites bound by biotinylated JQ1 are highly similar to the sites occupied by BRD2, BRD3 and BRD4 (**Fig. 1d,e**). This was further confirmed by inspection of data at individual genes with pivotal roles in myeloma biology, such as CCND2 (**Fig. 1f**). By contrast, a functionally inactive enantiomer of bio-JQ1 (bio-JQ1R, **Supplementary Fig. 3a**) did not produce significant Chem-seq signals (**Supplementary Fig. 3b,c**). These results indicate that both live-cell– and cell-lysate–based Chem-seq approaches (**Fig. 1a**) can be used to uncover the interactions of small molecules with their chromatin targets across the human genome. Of note, JQ1 is known to displace BET bromodomains from the genome, but the ability to detect the bio-JQ1/BRD complex on chromatin is likely made possible by covalent tethering of these proteins to chromatin during fixation (**Supplementary Fig. 4**).

We next investigated the extent to which Chem-seq and ChIP-seq signals overlap (**Fig. 2**). The pattern of JQ1 occupancy was best associated with the pattern of BRD4 occupancy (**Fig. 2a**). Pearson

correlation analysis also showed that bio-JQ1 signals were most highly correlated with BRD4, somewhat less frequently with BRD2 and much less frequently with BRD3 (**Fig. 2b**). We then developed a general linear model to identify genomic regions with differential signal between bio-JQ1 Chem-seq and each of the BRD ChIP-seq data sets. We found that bio-JQ1 co-occupied nearly all regions (>99%) with BRD4 genome-wide across triplicate data sets, bio-JQ1 and BRD2 co-occupied 96% of all genomic sites, and bio-JQ1 and BRD3 co-occupied 63% of all genomic sites (**Fig. 2c**). Inspection of gene tracks for regions differentially occupied by bio-JQ1 and the three BET proteins provided visual confirmation that bio-JQ1 tends to co-occupy enhancers where there are substantial BRD4 signals and lower signals for BRD2 and BRD3 (**Fig. 2d**). The pattern of BRD3 genome occupancy differed most from that of the other two BET proteins (**Fig. 2a–c**), because of pronounced signals at a subset of core promoter sites (**Fig. 2e**). Similar results were obtained with an alternative BRD3 ChIP antibody directed against a different epitope of this protein (**Supplementary Fig. 5**). Taken together, these results indicate that the pattern of JQ1 occupancy of chromatin is most strongly correlated with that of BRD4 in MM1.S cells,
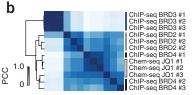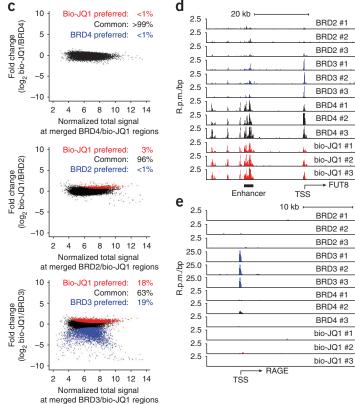
Figure 2 Genome-wide drug target analysis. (**a**) Genome-wide binding averages of BRD2, BRD3, BRD4 (ChIP-seq) and bio-JQ1 (*in vitro* Chem-seq) on active enhancers, active promoters and gene bodies in MM1.S cells. (**b**) Heatmap showing the similarity of signal distribution between bio-JQ1 (*in vitro* Chem-seq) and BET bromodomain proteins BRD2, BRD3 and BRD4 (ChIP-seq) by Pearson correlation at 25,693 genomic regions bound by BET proteins and bio-JQ1. Blue reflects high similarity of signal between each pair of factors. Factors are arranged and clustered along both axes based on the distance calculated from Pearson correlation. ChIP-seq and Chem-seq data for each factor were generated from three independent experiments. PCC, Pearson correlation coefficient. (**c**) Differential occupancy analysis of bio-Q1 (*in vitro* Chem-seq) and either BET bromodomain protein (ChIP-seq). The log ratios of normalized bio-JQ1 *in vitro* Chem-seq signal to BRD ChIP-seq signal are plotted for genomic regions identified as enriched for the presence of bio-JQ1 or either BRD protein. Triplicate ChIP-seq or Chem-seq data sets were used for each calculation. (**d**) Gene tracks showing the FUT8 enhancer, a site identified as bio-JQ1 high/BRD3 low region in (**c**, lower panel, red). Triplicate data sets were generated for each factor. (**e**) Gene tracks surrounding the transcriptional start site (TSS) of the PAGE gene, a 'BRD3 preferred region' (BRD3 high/bio-JQ1 low) identified in (**c**, lower panel, blue). R.p.m./bp, reads per million per base pair.

consistent with the relative affinities of JQ1 for these BET proteins previously established *in vitro*[27].

To extend the Chem-seq method to other drug classes, we initially focused on AT7519, an inhibitor of the cyclin-dependent kinase CDK9 (ref. 28), which is associated with the transcription apparatus at promoters. CDK9 phosphorylation of RNA Pol II and various transcription pause control factors stimulates active elongation[29]. We first confirmed that CDK9 co-occupies the promoters of active genes with RNA Pol II by using ChIP-seq (**Fig. 3a,b**). CDK9 is a core component of the positive transcription elongation factor, p-TEFb[29], and its inhibition would be expected to affect the levels of elongating RNA Pol II, which is located across the body of genes, to a much greater extent than the levels of initiating RNA Pol II, located at the transcription start site (TSS). Indeed, treatment of MM1.S cells with AT7519 was found to cause a reduction in the level of elongating RNA Pol II based on examination of individual gene tracks (**Fig. 3c**) and on analysis of the ratio of initiating versus elongating RNA Pol II molecules at active genes throughout the genome (**Fig. 3d**). We next generated a retrievable biotinylated derivative of AT7519 (**Fig. 3e**). The biotinylated compound did not enter cells as readily as AT7519 (**Fig. 3f,g**), so we used the *in vitro* Chem-seq method to investigate binding of bio-AT7519 to chromatin genome-wide. The results show that bio-AT7519 Chem-seq signals occur frequently at sites occupied by CDK9 (**Fig. 3h,i**). The bio-AT7519 Chem-seq signals were weaker than those observed for bio-JQ1, which may reflect differences in accessibility, association constants or ligand-receptor sensitivity to sample preparation. Nonetheless, there was a correlation between bio-AT7519 occupancy and CDK9 occupancy genome-wide (**Supplementary Fig. 6a**). There was also a substantial number of sites that were not co-occupied by bio-AT7519 and CDK9; it is possible that this was because of the relatively weak signals we obtained for bio-AT7519 Chem-seq or because AT7519
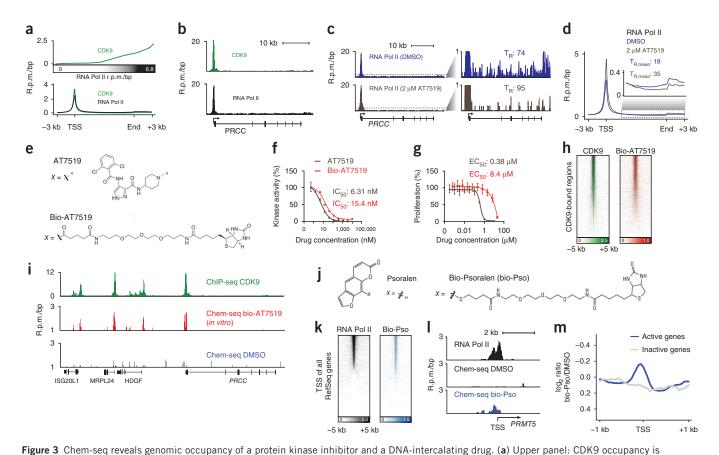
can inhibit other kinases[28,30] that may occupy other genomic sites (**Supplementary Fig. 6b**). Notably, a comparison of the Chem-seq data for bio-AT7519 and bio-JQ1 with ChIP-seq data for various components of the transcription apparatus (CDK7, CDK8, CDK9, RNA Pol II, Mediator and BRD4) revealed that bio-AT7519 was most often associated with CDK9, whereas bio-JQ1 was most often associated with BRD4 (**Supplementary Fig. 6c**). These results suggest that Chem-seq can be useful for identifying the genomic binding sites of kinase inhibitors.

To further extend the Chem-seq method to other drug classes, we investigated how the DNA intercalator psoralen interacts with genomic DNA *in vivo*. Recent studies have shown that psoralen preferentially intercalates at the TSS of active genes[31,32]. We used the *in vivo* Chem-seq method with biotinylated psoralen (bio-psoralen) (**Fig. 3j**) to explore this observation genome-wide in MM1.S cells. The results confirm that bio-psoralen preferentially binds to the TSS of active genes (**Fig. 3k–m**). Thus, Chem-seq can detect local enrichment of DNA intercalating agents throughout the human genome.

A broad range of drugs should generally be amenable to biotinylation and Chem-seq analysis. The design and synthesis of biotinylated probes can be informed by structural data from drug-target complexes; such X-ray structures allow the identification of suitable attachment positions that can be covalently linked to the biotin moiety and that remain freely accessible in the complex. Suitable attachment points could also be inferred from structure-activity relationship data derived from structurally related compounds. If such data are not available, several attachment sites can be selected for biotinylation, and the derived probes can be tested experimentally to see if they remain bound to the target. Points of attachment can either be provided by functional groups already present in the drug molecule or may be obtained through chemical modification of the compound structure, such as alkylation or addition of amide or ester linkages.

Figure 3 Chem-seq reveals genomic occupancy of a protein kinase inhibitor and a DNA-intercalating drug. (**a**) Upper panel: CDK9 occupancy is correlated with the RNA Pol II at promoters in MM1.S cells. Median CDK9 signal at promoters is ranked by increasing RNA Pol II occupancy. Signals are shown in units of reads per million per base pair (r.p.m./bp). Promoters were binned (50/bin) and a smoothing function was applied to median signals. Lower panel: genome-wide binding averages of CDK9 and RNA Pol II on active promoters and gene bodies in MM1.S cells as determined by ChIP-seq analysis. (**b**) Gene tracks showing occupancy of the PRCC gene by CDK9 and RNA Pol II based on ChIP-seq data. (**c**) Effect of AT7519 treatment on RNA Pol II occupancy at the *PRCC* gene. MM1.S cells were treated with either DMSO vehicle (blue) or 2 μM AT7519 (brown) for 6 h, followed by RNA Pol II ChIP-seq analysis. 20-fold magnifications of the r.p.m./bp scale of these gene tracks are shown in the right panel to show the difference in reads for elongating RNA Pol II. T_R, RNA Pol II traveling ratio. (**d**) Genome-wide binding average RNA Pol II (ChIP-seq) on active promoters and gene bodies following treatment of MM1.S cells with DMSO vehicle (blue) or 2 μM of AT7519 (brown) for 6 h. Magnification of the r.p.m./bp scale at gene bodies is shown in the inset. The inset includes RNA Pol II traveling ratio distributions ($T_{R,mean}$) derived from MM1.S cells treated with DMSO (blue) or 2 μM AT7519 (black). (**e**) Chemical structures of the pan-CDK inhibitor AT7519 and its biotinylated counterpart bio-AT7519. (**f**) *In vitro* kinase assays with recombinant cyclin T-CDK9 complex in the presence of increasing concentrations of AT7519 or bio-AT7519. The derived IC_{50} values for each compound are shown. (**g**) Effect of AT7519 and bio-AT7519 on MM1.S cell proliferation. Cells were treated with varying concentrations of drug for 72 h as indicated. The derived EC_{50} values for each compound are shown. Error bars are mean ± s.d. (**h**) Heatmap representation of CDK9 (ChIP-seq, green) and bio-AT7519 binding (*in vitro* Chem-seq, red) to all CDK9 occupied regions, rank ordered from highest to lowest CDK9 occupancy. Read density surrounds the center (±5 kb) of all occupied regions. (**i**) Gene tracks showing occupancy of the *PRCC* gene locus by bio-AT7519 (red) and DMSO (vehicle, blue) as assessed by *in vitro* Chem-seq analysis, and by CDK9 (ChIP-seq, green). (**j**) Chemical structures of psoralen and biotinylated psoralen. (**k**) Heatmap representation of RNA Pol II (ChIP-seq, black) and bio-psoralen binding (*in vivo* Chem-seq, light blue) to all human RefSeq genes, rank ordered from highest to lowest RNA Pol II occupancy. Read density surrounds the center (±5 kb) of occupied regions. (**l**) Gene tracks centered at the TSS of the *PRMT5* gene, showing occupancy of bio-psoralen (bottom panel, light blue) versus DMSO (middle panel) as revealed by *in vivo* Chem-seq analysis, together with RNA Pol II ChIP-seq data (upper panel, black). (**m**) Representation of bio-psoralen *in vivo* Chem-seq data at ±1 kb around the TSS of active (light blue) and inactive (gray) genes. Log₂ ratio of the mean bio-psoralen Chem-seq signal to mean DMSO signal in 50-bp bins is plotted.

Finally, as there is an expanding interest in elucidating the mechanisms of action of many drugs, biotinylated versions of such compounds are increasingly becoming commercially available.

In summary, Chem-seq provides a method to identify the sites bound by small chemical molecules throughout the genome. When combined with other global analysis methods such as ChIP-seq, Chem-seq provides an approach to investigate the direct, genome-wide effects of therapeutic modalities. Mapping the global interactions of a chemical entity with chromatin genome-wide should provide insights into the mechanisms by which small molecules perturb gene expression programs.

METHODS

Methods and any associated references are available in the online version of the paper.

Accession codes. Chem-seq and ChIP-seq data, GEO: GSE44098 and GSE43743, respectively. The QC metrics for Chem-seq data sets are summarized in **Supplementary Table 1**.

Note: Any Supplementary Information and Source Data files are available in the online version of the paper.

AUTHOR CONTRIBUTIONS

J.J.M., P.B.R., J.E.B. and R.A.Y. conceived of the Chem-seq method, L.A. and M.G.G. developed the method, L.A. generated bio-JQ1 and bio-psoralen Chem-seq data, M.G.G. generated bio-AT7519 Chem-seq data, Z.P.F. developed computational methods and analyzed the data, J.Q. and J.J.M. synthesized biotinylated derivatives of chemical probes, J.Q. performed protein biochemistry, L.A. generated ChIP-seq data for BRD2, BRD3, BRD4, CDK7, CDK8, H4K20me3 and H3K27me3, P.B.R. and J.L. generated ChIP-seq data for RNA Pol II and CDK9, W.B.S. generated cellular proliferation data, A.A.S. contributed to optimize Chem-seq, T.I.L. provided advice on method development, and J.E.B. and R.A.Y. supervised the research.

COMPETING FINANCIAL INTERESTS

The authors declare competing financial interests: details are available in the online version of the paper.

Reprints and permissions information is available online at http://www.nature.com/reprints/index.html.

1. Bell, O., Tiwari, V.K., Thoma, N.H. & Schubeler, D. Determinants and dynamics of genome accessibility. *Nat. Rev. Genet.* **12**, 554–564 (2011).
2. Gilbert, D.M. Evaluating genome-scale approaches to eukaryotic DNA replication. *Nat. Rev. Genet.* **11**, 673–684 (2010).
3. Hawkins, R.D., Hon, G.C. & Ren, B. Next-generation genomics: an integrative approach. *Nat. Rev. Genet.* **11**, 476–486 (2010).
4. MacQuarrie, K.L., Fong, A.P., Morse, R.H. & Tapscott, S.J. Genome-wide transcription factor binding: beyond direct target regulation. *Trends Genet.* **27**, 141–148 (2011).
5. Neph, S. *et al.* Circuitry and dynamics of human transcription factor regulatory networks. *Cell* **150**, 1274–1286 (2012).
6. Zhou, V.W., Goren, A. & Bernstein, B.E. Charting histone modifications and the functional organization of mammalian genomes. *Nat. Rev. Genet.* **12**, 7–18 (2011).
7. Ng, H.H. & Surani, M.A. The transcriptional and signalling networks of pluripotency. *Nat. Cell Biol.* **13**, 490–496 (2011).
8. Northrup, D.L. & Zhao, K. Application of ChIP-Seq and related techniques to the study of immune function. *Immunity* **34**, 830–842 (2011).
9. Orkin, S.H. & Hochedlinger, K. Chromatin connections to pluripotency and cellular reprogramming. *Cell* **145**, 835–850 (2011).
10. Young, R.A. Control of the embryonic stem cell state. *Cell* **144**, 940–954 (2011).
11. Arrowsmith, C.H., Bountra, C., Fish, P.V., Lee, K. & Schapira, M. Epigenetic protein families: a new frontier for drug discovery. *Nat. Rev. Drug Discov.* **11**, 384–400 (2012).
12. Copeland, R.A., Solomon, M.E. & Richon, V.M. Protein methyltransferases as a target class for drug discovery. *Nat. Rev. Drug Discov.* **8**, 724–732 (2009).
13. Dawson, M.A. *et al.* Inhibition of BET recruitment to chromatin as an effective treatment for MLL-fusion leukaemia. *Nature* **478**, 529–533 (2011).
14. Deshpande, A.J., Bradner, J. & Armstrong, S.A. Chromatin modifications as therapeutic targets in MLL-rearranged leukemia. *Trends Immunol.* **33**, 563–570 (2012).
15. Sandoval, J. & Esteller, M. Cancer epigenomics: beyond genomics. *Curr. Opin. Genet. Dev.* **22**, 50–55 (2012).
16. You, J.S. & Jones, P.A. Cancer genetics and epigenetics: two sides of the same coin? *Cancer Cell* **22**, 9–20 (2012).
17. Raida, M. Drug target deconvolution by chemical proteomics. *Curr. Opin. Chem. Biol.* **15**, 570–575 (2011).
18. Bantscheff, M. *et al.* Chemoproteomics profiling of HDAC inhibitors reveals selective targeting of HDAC complexes. *Nat. Biotechnol.* **29**, 255–265 (2011).
19. Ito, T. *et al.* Identification of a primary target of thalidomide teratogenicity. *Science* **327**, 1345–1350 (2010).
20. Taunton, J., Hassig, C.A. & Schreiber, S.L. A mammalian histone deacetylase related to the yeast transcriptional regulator Rpd3p. *Science* **272**, 408–411 (1996).
21. Tung, S.Y., Hong, J.Y., Walz, T., Moazed, D. & Liou, G.G. Chromatin affinity-precipitation using a small metabolic molecule: its application to analysis of O-acetyl-ADP-ribose. *Cell. Mol. Life Sci.* **69**, 641–650 (2012).
22. Chung, C.W. *et al.* Discovery and characterization of small molecule inhibitors of the BET family bromodomains. *J. Med. Chem.* **54**, 3827–3838 (2011).
23. Delmore, J.E. *et al.* BET bromodomain inhibition as a therapeutic strategy to target c-Myc. *Cell* **146**, 904–917 (2011).
24. Filippakopoulos, P. *et al.* Selective inhibition of BET bromodomains. *Nature* **468**, 1067–1073 (2010).
25. Loven, J. *et al.* Selective inhibition of tumor oncogenes by disruption of super-enhancers. *Cell* **153**, 320–334 (2013).
26. Nicodeme, E. *et al.* Suppression of inflammation by a synthetic histone mimic. *Nature* **468**, 1119–1123 (2010).
27. Zuber, J. *et al.* RNAi screen identifies Brd4 as a therapeutic target in acute myeloid leukaemia. *Nature* **478**, 524–528 (2011).
28. Santo, L. *et al.* AT7519, A novel small molecule multi-cyclin-dependent kinase inhibitor, induces apoptosis in multiple myeloma via GSK-3beta activation and RNA polymerase II inhibition. *Oncogene* **29**, 2325–2336 (2010).
29. Zhou, Q., Li, T. & Price, D.H. RNA polymerase II elongation control. *Annu. Rev. Biochem.* **81**, 119–143 (2012).
30. Squires, M.S. *et al.* AT7519, a cyclin-dependent kinase inhibitor, exerts its effects by transcriptional inhibition in leukemia cell lines and patient samples. *Mol. Cancer Ther.* **9**, 920–928 (2010).
31. Kouzine, F. *et al.* Transcription-dependent dynamic supercoiling is a short-range genomic force. *Nat. Struct. Mol. Biol.* **20**, 396–403 (2013).
32. Naughton, C. *et al.* Transcription forms and remodels supercoiling domains unfolding large-scale chromatin structures. *Nat. Struct. Mol. Biol.* **20**, 387–395 (2013).

ONLINE METHODS

Compounds. AT7519 and biotinylated psoralen (EZ-Link Psoralen-PEG-Biotin) were obtained from Selleck Chemicals and Thermo Fisher Scientific, respectively. Biotinylated JQ1 (bio-JQ1) and biotinylated AT7519 (bio-AT7519) were synthesized as described in **Supplementary Methods**.

Cell culture and treatment with unbiotinylated drugs. MM1.S cells (CRL-2974, ATCC) were maintained in RPMI-1640 supplemented with 10% FBS and 1% GlutaMAX (Invitrogen, 35050-061). For JQ1 treatment experiments, asynchronous cells were treated with varying concentrations of JQ1 or vehicle (DMSO) for 6 h. Alternatively, cells were treated with 2 µM AT7519 for 6 h.

Genome-wide occupancy analysis of drug target proteins (ChIP-seq). ChIP coupled with massively parallel DNA sequencing (ChIP-seq) was performed as previously described[33]. The following antibodies were used for ChIP: anti-BRD4 (Bethyl Labs, A301-985A), anti-BRD2 (Cell signaling, 5848), anti-BRD3 (Bethyl Labs, A302-367A and A302-368A), anti-MED1 (Bethyl Labs, A300-793A), anti-H3K27Ac (Abcam, ab4729), anti-RNA-Pol II (Santa Cruz, sc-899), anti-CTCF (Millipore, 07-729) and anti-CDK9 (sc-484). For each ChIP, 10 µg of antibody was added to 3 ml of sonicated nuclear extract. Illumina sequencing, library construction and ChIP-seq analysis methods were previously described[33].

Expression of recombinant BRD4(1). The first bromodomain of BRD4 was purified as a poly-histidine-tagged recombinant human protein expressed in *Escherichia coli*, as previously described[24].

Differential scanning fluorimetry. Thermal melting experiments were carried out using a 7300 Real Time PCR machine (AB Applied Biosystems). Proteins were buffered in 10 mM HEPES pH 7.5, 500 mM NaCl and assayed in a 96-well plate at a final concentration of 1 µM in 20-µl volume. Compounds were added at a final concentration of 10 µM. SYPRO Orange (Molecular Probes) was added as a fluorescence probe at a dilution of 1:1,000. Excitation and emission filters for the SYPRO-Orange dye were set to 465 nm and 590 nm, respectively. The temperature was raised with a step of 4 °C per minute from 25 °C to 96 °C and fluorescence readings were taken at each interval. The observed temperature shifts, ΔTm obs, were recorded as the difference between the transition midpoints of sample and reference (DMSO) wells containing protein without ligand in the same plate.

Isothermal titration calorimetry (ITC). ITC was performed using an ITC200 microcalorimeter from MicroCal (Northampton, MA). All experiments were carried out at 25 °C while stirring at 1,000 r.p.m., in ITC buffer (50 mM HEPES pH 7.4 at 25 °C, 150 mM NaCl). The microsyringe was loaded with a solution of the protein sample (190 µM, in ITC buffer). All titrations were conducted using an initial injection of 0.2 µl, followed by 19 identical injections of 2 µl with a duration of 5 s (per injection) and a spacing of 90 s between injections. The heat of dilution was determined by independent titrations (protein into buffer) and was subtracted from the experimental data. The collected data were implicated in the MicroCal Origin software supplied with the instrument to yield enthalpies of binding (ΔH) and binding constants. A single binding site model was employed. Dissociation constants and thermodynamic parameters are presented in **Supplementary Figure 2c**.

***In vivo* genome-wide occupancy analysis of biotinylated JQ1 (*in vivo* Chem-seq).** Exponentially growing MM1.S cells (2 × 10^{8} cells per sample) were treated simultaneously with either 5 µM biotinylated JQ1 (Bio-JQ1) or DMSO (vehicle) and 1% formaldehyde for 20 min in cell culture medium. Chemical cross-linking was terminated by addition of TRIS buffer, pH 7.5, to a final concentration of 300 mM TRIS. Cells were harvested using a silicon scraper, centrifuged, and the derived pellets washed three times with PBS. Cell nuclei were prepared as follows: cells were lysed in 50 mM HEPES, pH 7.5, 140 mM NaCl, 1 mM EDTA, 10% glycerol, 0.5% NP-40, 0.25% Triton X-100 plus protease inhibitor cocktail 'complete' (Roche), and cell nuclei were washed once with 10 mM Tris-HCL, pH 8.0, 200 mM NaCl, 1 mM EDTA, 0.5 mM EGTA and protease inhibitors. Nuclei were resuspended and sonicated in 50 mM HEPES-KOH, pH 7.5, 140 mM NaCl, 1 mM EDTA, 1 mM EGTA,

1% Triton X-100, 0.1% Na-deoxycholate, 0.1% SDS (sonication buffer) and protease inhibitor cocktail at 18 W for 10 cycles (30 s each) on ice with 30-s intervals between cycles. Sonicated lysates were cleared by centrifugation and incubated for 16–20 h at 4 °C with magnetic streptavidin Dynabeads (MyOne Streptavidin T1, Invitrogen) (beads were blocked in PBS containing 0.5% BSA before this incubation step). Following incubation in nuclear sonicated lysate, beads were washed twice in sonication buffer, once in sonication buffer containing 500 mM NaCl, once in LiCl buffer (20 mM Tris-HCL, pH 8.0, 1 mM EDTA, 250 mM LiCl, 0.5% NP-40, 0.5% Na-deoxycholate), and once in 10 mM TRIS, pH 7.5, 0.1 mM EDTA. Bound protein-DNA complexes were subsequently eluted in 50 mM Tris-HCL, pH 8.0, 10 mM EDTA, 10% SDS at 65 °C for 15 min, and cross-links were reversed by overnight incubation of the eluate at 65 °C. Contaminating RNA and protein were digested by addition of RNase and Proteinase K, respectively, and the DNA purified as previously described[34]. Finally, purified DNA fragments were massively parallel sequenced and the sequencing data analyzed as described[33].

***In vitro* genome-wide occupancy analysis of biotinylated JQ1 (*in vitro* Chem-seq).** Exponentially growing, untreated MM1.S cells were fixed with 1% formaldehyde for 20 min in cell culture medium. Chemical cross-linking was terminated, cell nuclei prepared and sonicated nuclear lysate obtained as described above. Unlike in the *in vivo* protocol, however, Streptavidin Dynabeads were pre-incubated in PBS containing 0.5% BSA and either 200 µM biotinylated drug or vehicle (DMSO) for 6 h. Drug-bound beads were subsequently washed four times in PBS/0.5% BSA to remove unbound drug, and incubated in nuclear sonicated lysate for 16–20 h at 4 °C. All the following steps are identical to those described above (*in vivo* Chem-seq method).

***In vitro* genome-wide occupancy analysis using biotinylated AT7519 (*in vitro* Chem-seq).** Exponentially growing, untreated MM1.S cells were fixed with 0.5% formaldehyde for 5 min in cell culture medium. Chemical cross-linking was terminated by addition of TRIS buffer, pH 7.5, to a final concentration of 300 mM TRIS. Cells were washed 3× in PBS and cell nuclei prepared as follows: cell nuclei were lysed in 50 mM HEPES, pH 7.5, 140 mM NaCl, 1 mM EDTA, 10% glycerol, 0.5% NP-40, 0.25% Triton X-100 plus protease inhibitor cocktail 'complete' (Roche), and cell nuclei were washed once with 10 mM Tris-HCl, pH 8.0, 200 mM NaCl, 1 mM EDTA, 0.5 mM EGTA and protease inhibitors. Nuclei were resuspended and sonicated in 50 mM HEPES-KOH, pH 7.5, 140 mM NaCl, 1 mM EDTA, 1 mM EGTA, 0.5% NP-40, 0.5% Triton-X (sonication buffer). Pellets were sonicated at 9–12 W for 4 cycles (30 s each) in a Misonix sonicator on ice with 1-min rest intervals between cycles. Drug-bound beads were added to the cleared sonicate and the precipitation allowed to proceed for 12–18 h. Drug-bound beads were subsequently washed four times in sonication buffer, proteins eluted in 1% SDS, and cross-links were reversed by overnight incubation of the eluate at 65 °C in 1% SDS. Contaminating RNA and protein were digested by sequential incubation with RNase A and Proteinase K, and the DNA purified as previously described[34]. Purified DNA fragments were subjected to massively parallel sequencing (Illumina) and the sequencing data analyzed as described[33].

Genome-wide occupancy analysis of biotinylated psoralen by Chem-seq. Cell nuclei were prepared from exponentially growing MM.S cells using the Nuclei EZ prep kit (Sigma). Nuclei were then resuspended in ice-cold PBS and directly incubated with 5 µM biotinylated psoralen or vehicle (DMSO) for 30 min at 4 °C. Nuclei were washed once in PBS and immediately irradiated at 360 nm for 30 min (Stratalinker) on ice. Nuclei were resuspended and sonicated in 50 mM HEPES-KOH, pH 7.5, 140 mM NaCl, 1 mM EDTA, 1 mM EGTA, 1% Triton X-100, 0.1% Na-deoxycholate, 0.1% SDS (sonication buffer) and protease inhibitor cocktail at 18 W for 10 cycles (30 s each) on ice with 30 s intervals between cycles. Sonicated lysates were cleared by centrifugation and incubated for 16–20 h at 4 °C with magnetic Streptavidin Dynabeads (MyOne Streptavidin T1, Invitrogen) (beads were blocked in PBS containing 0.5% BSA before this incubation step). Following incubation in nuclear-sonicated lysate, beads were washed twice in sonication buffer, once in sonication buffer containing 500 mM NaCl, once in LiCl buffer (20 mM Tris-HCL, pH 8.0, 1 mM EDTA, 250 mM LiCl, 0.5% NP-40, 0.5% Na-deoxycholate), and once in 10 mM TRIS, pH 7.5, 0.1 mM EDTA. Bound protein-DNA complexes were

subsequently eluted in 50 mM Tris-HCL, pH 8.0, 10 mM EDTA, 10% SDS and 10 mM Biotin, and the eluate incubated o/n at 65 °C. Contaminating RNA and protein were digested by addition of RNase and Proteinase K, respectively, and the DNA purified as previously described[34]. Finally, purified DNA samples were irradiated at 254 nm for 5 min (Stratalinker) to reverse psoralen-DNA cross-links, followed by library preparation, massively parallel DNA sequencing and analysis of sequencing data[33].

Chem-seq and ChIP-seq data analysis. All ChIP-seq and Chem-seq data sets were aligned using Bowtie (version 0.12.2)[35] to build version NCBI36/HG18 of the human genome. We used the MACS version 1.4.1 (Model-based analysis of ChIP-seq)[36] peak finding algorithm to identify regions of ChIP-seq enrichment over background. A *P*-value threshold of enrichment of 1e-9 was used for all data sets except for Chem-seq bioAT7519 (1e-6). To obtain the normalized read density of ChIP-seq data sets in any region, ChIP-seq reads aligning to each region were extended automatically by MACS, and the density of reads per bp was calculated. The density of reads in each region was normalized to the total number of million mapped reads producing read density in units of reads per million mapped reads per bp (r.p.m./bp).

Definition of transcribed genes. A gene was defined as transcribed if an enriched region for either H3K4me3 or RNA Pol II was located within ± 5 kb of the TSS. H3K4me3 is a histone modification associated with transcription initiation[37].

Definition of active enhancers. Active enhancers were defined as regions of enrichment for H3K27Ac outside of promoters (greater than 2.5 kb away from any TSS). H3K27Ac is a histone modification associated with active enhancers[38,39]. Active enhancers form loops with promoters that are facilitated by the Mediator complex[40]. Thus, we validated H3K27Ac definitions of enhancers using ChIP-seq data for the mediator subunit Med1. Enriched regions from Med1 had >90% overlap with H3K27Ac regions in all data sets.

Determination of RNA Pol II traveling ratio. We determined the ratio of RNA Pol II ChIP-seq levels in initiating to elongating regions, a measure known as the traveling ratio (TR) (**Fig. 3c,d**)[41]. We defined the initiating region as ±300 bp around the TSS. We defined the elongating region as +300 bp from the TSS to +3,000 bp after the gene end. In order to make higher-confidence comparisons, we limited our analysis to genes with detectable signal above noise in the initiating and elongating regions across all samples. The statistical significance of changes in the distribution of traveling ratios was determined using two-tailed *t* test.

Heatmap representation of read density profiles. The enriched regions, the merged regions, or the annotated TSS of all RefSeq genes were aligned at the center in the composite view of signal density profile. The average ChIP-seq or Chem-seq read density (r.p.m./bp) around ±5 kb centered on the centers in 50 bp bin was calculated. The enriched regions of BRD2, BRD3 and BRD4 ChIP-seq and bio-JQ1 Chem-seq were merged together if overlapping by 1 bp, resulting in a total of 25,450 merged regions. For bio-psoralen Chem-seq analysis, the annotated TSS of all RefSeq genes were used.

Pairwise comparison between Chem-seq and ChIP-seq. The set of genomic regions that were enriched for Chem-seq or ChIP-seq signal used in pairwise comparisons were merged together if overlapping by 1 bp. The average ChIP-seq or Chem-seq read density was calculated in reads per million mapped reads per bp (r.p.m./bp) for each of the merged regions. The pair-wise comparisons by Pearson correlation were performed on all data sets using the average read density at the merged regions. The average linkage hierarchical clustering of the Pearson correlation was shown in the heatmap (**Supplementary Figs. 2b**, **5a** and **6c**). For **Figure 2b**, the enriched regions of 3 replicate JQ1 *in vitro* Chem-seq data sets, 3 replicate BRD2 ChIP-seq data sets, 3 replicate BRD3 ChIP-seq data sets, and 3 replicate BRD4 ChIP-seq data sets were merged together, resulting a total of 29,693 merged regions. For **Supplementary Figure 5a**, the enriched regions of bio-JQ1 (*in vitro* Chem-seq), BRD2, BRD3 from two different antibodies, and BRD4 (ChIP-seq) were merged together, resulting a total of 25,693 merged regions. For **Supplementary Figure 6c**, the enriched regions of

CDK7, CDK8, CDK8, BRD4, MED1, RNA Pol II, H3K20me3 and H3K27me3 were merged together, resulting a total of 50,638 merged regions.

Specificity analysis based on overlap between Chem-seq and ChIP-seq data. We analyzed Chem-seq and ChIP-seq data to identify genomic regions with substantial JQ1 Chem-seq signal but no significant BRD2, BRD3 or BRD4 ChIP-seq signal and vice versa (**Fig. 2b**). We adopted a general linear model to identify regions with differential signal between JQ1 and BET proteins[42,43]. We first identified the set of genomic regions that were enriched for JQ1 Chem-seq or BET protein ChIP-seq signal in any one of the 12 data sets being considered (3 replicate JQ1 vitro Chem-seq data sets, 3 replicate BRD2 ChIP-seq data sets, 3 replicate BRD3 ChIP-seq data sets and 3 replicate BRD4 ChIP-seq data sets). Regions from a data set that overlapped with regions from another data set by 1 bp were merged together to form a representative region that spans the combined genomic region. A total of 29,693 regions were identified. For each region, the read density in reads per million per base pair (r.p.m./bp) was calculated, and from this the relative read count of each region was obtained by multiplying read density by the length of the region. The *edgeR* package was used to model technical variation due to noise among triplicate data sets and the biological variation due to differences in signal between JQ1 Chem-seq and BET protein ChIP-seq data sets[42]. Sequencing depth and upper-quantile techniques were used to normalize all 12 data sets together before common and tagwise dispersions were estimated. The statistical significance of differences between JQ1 Chem-seq signals and each of BET protein ChIP-seq signals was next calculated using an exact test and resulting *P* values were subjected to Benjamini–Hochberg multiple testing correction (FDR). For robustness, only regions where all triplicates showed significant enrichment of either ChIP-seq or Chem-seq signal (signal in units of r.p.m./bp above bottom 5 percentiles of enriched regions) were used for differential signal analyses. This resulted in only 16,266, 17,556 and 17,802 regions being further considered in the pair-wise comparisons of BRD2 vs. JQS, BRD3 vs. JQS, and BRD4 vs. JQS, respectively. We only detect only one region showing substantially more JQ1 Chem-seq signal than BRD4 ChIP-seq signal. However, this region did have enrichment of BRD4 ChIP-seq. These data indicate that, under these experimental conditions, there is no identifiable off-target interaction that results in JQ1 Chem-seq signal at regions of the genome without BRD4.

Cyclin T1-CDK9 *in vitro* kinase assay. Life Technologies SelectScreen Profiling service was used to obtain IC$_{50}$ values for inhibition by AT7519 versus biotinylated AT7519.

Composite biotinylated psoralen (bio-psoralen) occupancy profile. The TSS of active and inactive genes were aligned at the center in the composite view of bio-psoralen enrichment. The average Chem-Seq read density of bio-psoralen and DMSO control around ±1 kb centered on the TSS in a 50-bp bin was calculated in r.p.m./bp. The log$_2$ ratio of mean signal of bio-psoralen and DMSO in 50-bp bins is plotted.

33. Marson, A. *et al.* Connecting microRNA genes to the core transcriptional regulatory circuitry of embryonic stem cells. *Cell* **134**, 521–533 (2008).
34. Lee, T.I., Johnstone, S.E. & Young, R.A. Chromatin immunoprecipitation and microarray-based analysis of protein location. *Nat. Protoc.* **1**, 729–748 (2006).
35. Langmead, B., Trapnell, C., Pop, M. & Salzberg, S.L. Ultrafast and memory-efficient alignment of short DNA sequences to the human genome. *Genome Biol.* **10**, R25 (2009).
36. Zhang, Y. *et al.* Model-based analysis of ChIP-Seq (MACS). *Genome Biol.* **9**, R137 (2008).
37. Guenther, M.G., Levine, S.S., Boyer, L.A., Jaenisch, R. & Young, R.A. A chromatin landmark and transcription initiation at most promoters in human cells. *Cell* **130**, 77–88 (2007).
38. Rada-Iglesias, A. *et al.* A unique chromatin signature uncovers early developmental enhancers in humans. *Nature* **470**, 279–283 (2011).
39. Creyghton, M.P. *et al.* Histone H3K27ac separates active from poised enhancers and predicts developmental state. *Proc. Natl. Acad. Sci. USA* **107**, 21931–21936 (2010).
40. Kagey, M.H. *et al.* Mediator and cohesin connect gene expression and chromatin architecture. *Nature* **467**, 430–435 (2010).
41. Rahl, P.B. *et al.* c-Myc regulates transcriptional pause release. *Cell* **141**, 432–445 (2010).
42. Robinson, M.D., McCarthy, D.J. & Smyth, G.K. edgeR: a Bioconductor package for differential expression analysis of digital gene expression data. *Bioinformatics* **26**, 139–140 (2010).
43. Ross-Innes, C.S. *et al.* Differential oestrogen receptor binding is associated with clinical outcome in breast cancer. *Nature* **481**, 389–393 (2012).